ACS APPLIED MATERIALS & INTERFACES

Research Article

www.acsami.org

Surface-Directed Synthesis of Erbium-Doped Yttrium Oxide Nanoparticles within Organosilane Zeptoliter Containers

Lauren E. Englade-Franklin,[†] Gregory Morrison,[†] Susan D. Verberne-Sutton,[†] Asenath L. Francis,[†] Julia Y Chan,[‡] and Jayne C. Garno*[,†]

[†]Department of Chemistry, Louisiana State University, Baton Rouge, Louisiana 70803, United States

[‡]Department of Chemistry, University of Texas, Richardson, Texas 75080, United States

Supporting Information

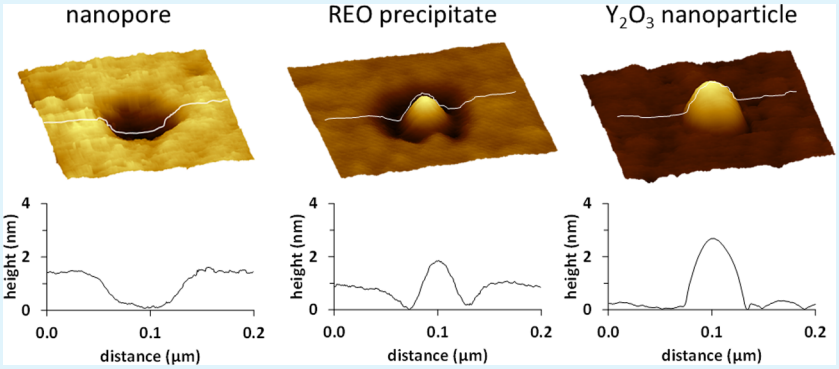

ABSTRACT: We introduce an approach to synthesize rare earth oxide nanoparticles using high temperature without aggregation of the nanoparticles. The dispersity of the nanoparticles is controlled at the nanoscale by using small organosilane molds as reaction containers. Zeptoliter reaction vessels prepared from organosilane self-assembled monolayers (SAMs) were used for the surface-directed synthesis of rare earth oxide (REO) nanoparticles. Nanopores of octadecyltrichlorosilane were prepared on Si(111) using particle lithography with immersion steps. The nanopores were filled with a precursor solution of erbium and yttrium salts to confine the crystallization step to occur within individual zeptoliter-sized organosilane reaction vessels. Areas between the nanopores were separated by a matrix film of octadecyltrichlorosilane. With heating, the organosilane template was removed by calcination to generate a surface array of erbium-doped yttria nanoparticles. Nanoparticles synthesized by the surface-directed approach retain the periodic arrangement of the nanopores formed from mesoparticle masks. While bulk rare earth oxides can be readily prepared by solid state methods at high temperature (>900 °C), approaches for preparing REO nanoparticles are limited. Conventional wet chemistry methods are limited to low temperatures according to the boiling points of the solvents used for synthesis. To achieve crystallinity of REO nanoparticles requires steps for high-temperature processing of samples, which can cause self-aggregation and dispersity in sample diameters. The facile steps for particle lithography address the problems of aggregation and the requirement for high-temperature synthesis.

KEYWORDS: *nanoparticle synthesis, rare earth oxide, organosilanes, particle lithography, surface template synthesis, luminescence*

INTRODUCTION

The optical, catalytic, and magnetic properties of bulk materials of rare earth oxides (REO) have been applied commercially in optical displays, alternatives for catalytic converters, or as permanent magnets in disk drives.[1−5] The current challenge for synthesizing nanomaterials with rare earth elements requires synthetic capabilities to achieve high crystallinity and monodispersity of the products. Heating at temperatures in the range of 900−1400 °C is necessary to produce crystalline REO nanomaterials.[6] The properties of REO materials greatly depend on achieving a high degree of crystallization for samples.[7] Wet chemistry approaches that are commonly used for preparing metal nanoparticles are not amenable for synthesis with such high temperatures. Methods such as postannealing to obtain crystallinity for nanomaterials tend to cause sintering of the nanoparticles, and capping agents used to control the shape and size may interfere with the desired catalytic or optical properties of the nanoparticles.[8,9] To address the limitations of solution-based methods, we have developed a surface-directed procedure for high-temperature synthesis, using nanopores within organic films as reaction containers. The matrix film provides a surface platform to spatially segregate small volumes of reagents, which is efficiently removed by calcination during heating steps.

At the microscale, the strategy of using a surface template to mold and form nanomaterials has previously been investigated

Received: June 6, 2014
Accepted: August 28, 2014
Published: August 28, 2014

for precipitation of salts and protein solutions. Surface arrangements of microcrystals of (KBr, KH_2PO_4, NaCl, KNO_3, $NaNO_3$, hydroquinone, and glycine) were prepared within micropatterned photoresists by Thalladi et al.[10] Micropatterned wells prepared by photolithography were functionalized with thiol chemistry for the crystallization of proteins by Wang et al.[11] Crystals of calcite were grown within micropatterned self-assembled monolayers (SAMs) prepared by microcontact printing by Aizenburg et al.[12] Using templates prepared with microcontact printing of SAMs, magnetic nanoparticles (cobalt, nickel, ferrites) ranging from 70 to 460 nm in size were prepared on silicon substrates from nitrate salt deposits after heating to 600 °C, demonstrated by Zhong et al.[13] Defined arrangements of magnetic colloids were prepared at the micron scale on glass surfaces by Lyles et al. using a process of polymer-on-polymer stamping with microcontact printing.[14] Arrays of gold nanoparticles were fabricated on ITO substrates using a method that combined nanoimprint lithography with electrochemical deposition by Ma et al.[15] The crystals produced with methods of photolithography and microcontact printing have the additional advantage of being prepared with well-defined arrangements on surfaces.

Nanoscale patterning of SAMs can be accomplished with particle lithography without using manufactured molds or masks prepared with electron beams to achieve small features.[16−18] Particle lithography can be used to prepare surface molds of SAMs to define sites for the deposition of nanomaterials and to provide spatial separation during subsequent steps of drying or heating. The photoluminescent properties of $NaYF_4$:Yb,Er rare earth nanoparticles prepared using particle lithography to generate periodically arranged rings of nanoparticles was investigated by Mullen et al.[19] Nanorings of *n*-octadecyltrichlorosilane (OTS) were used as sites to nucleate nanoparticles of small organic molecules such as *n*-docosane, aspirin, and clarithromycin prepared using particle lithography by Wang et al.[20]

Erbium-doped yttrium oxide nanoparticles have interesting luminescent properties such as intense cathodoluminescence and photoluminescence.[7,21] Nanomaterials of yttrium oxide doped with rare earth elements have been prepared by flame spray pyrolysis (Eu:Y_2O_3),[7] thermal decomposition of a polymeric resin,[22] atomic layer deposition,[23] gas-phase condensation,[24] flux,[25] combustion,[26−28] solvothermal[29] and hydrothermal methods,[30−36] alkalide reduction,[37] solution-based sol−gel processes,[38] emulsion techniques,[39−41] precipitation,[42−44] and electrochemical[45] methods. Preparation of Y_2O_3:Eu^{3+} nanowires using a template of anodized aluminum oxide that was heated to 800 °C was reported by Zhang et al.[44] Ordered arrays of Y_2O_3:Eu^{3+} nanotubes were prepared in anodic alumina membranes by a method of electronic field-assisted deposition.[46]

In this report, nanopores within organosilane self-assembled monolayers (SAMs) that were prepared using particle lithography were used as containers for the surface-directed synthesis of erbium-doped yttrium oxide nanoparticles at high temperatures. The sacrificial surface mold of octadecyltrichlorosilane (OTS) was used to define the deposition of precipitates of rare earth salts from solution as a means to control the size, dispersity and surface density. Successive heating steps were used to crystallize the rare earth oxide (REO) deposits as well as to remove the OTS resist. Our goal was to produce spatially separated nanoparticles of erbium-doped yttrium oxide with a periodicity defined by surface masks of silica mesospheres. Micropatterns that were prepared by capillary filling of polydimethylsiloxane (PDMS) molds provided an approach to optimize the heating protocol for converting yttrium salt precipitates into yttrium oxide. The analysis of sample morphologies, surface density and periodicity was accomplished with atomic force microscopy (AFM).

EXPERIMENTAL SECTION

Preparation of Yttrium Precursor Solution. A rare earth salt solution comprising yttrium trichloroacetic acid was prepared according to a previously published procedure.[47] Yttria powder (15 mmol) was dissolved in concentrated nitric acid (100 mL) by heating to 80 °C. After the solid had dissolved, the salt solution was cooled to room temperature. Yttrium hydroxide was then precipitated from solution by adding NH_4OH until basic. The precipitate was isolated by vacuum filtration, washed several times with cold deionized water, and air-dried. A solution of yttrium trichloroacetic acid was prepared by dissolving the hydroxide precipitate in a 25% trichloroacetic acid solution. Just enough of the acid was added to dissolve the precipitate to make a saturated solution of the salt. A second solution was prepared at half of the concentration of the original solution to study the effect of concentration on the size of the nanoparticles.

Micropatterns Prepared by Capillary Filling of PDMS molds. Micrometer-scale patterns of Y_2O_3 were fabricated to provide surface structures for XRD characterizations. Microline patterns of yttrium oxide were prepared from the saturated yttrium salt solution to optimize the heating parameters for yttria synthesis. The method of capillary filling of PDMS molds has been previously demonstrated with solutions of proteins.[48−50] The capillary filling of microchannels of PDMS molds is also suitable for directing the placement of salt solutions on flat surfaces. Detailed steps for the procedure of capillary filling of PDMS molds are provided in the Supporting Information, Figure S1.

Nanoparticles of Er-doped Y_2O_3. The procedure for preparing nanoparticles of erbium-doped yttria on a silicon surface is outlined in Figure 1. Octadecyltrichlorosilane (OTS) molecules were deposited on a silicon substrate using immersion particle lithography to form nanopores (Figure 1a), as previously reported.[18] The nanoscopic

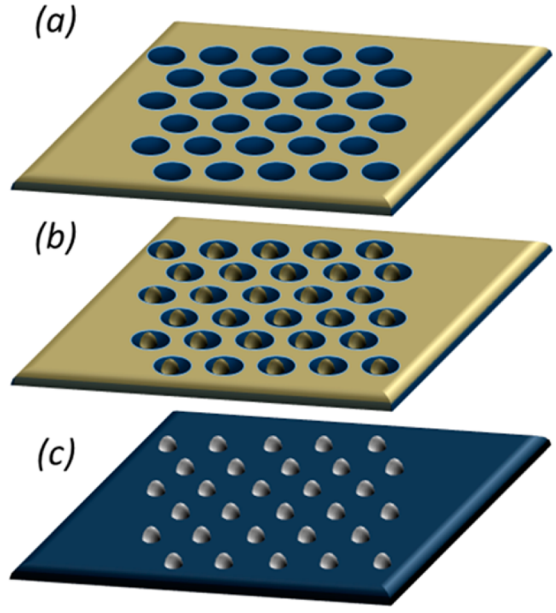

Figure 1. Basic steps to prepare a surface array of REO nanoparticles. (a) Sacrificial template of organosilane nanopores prepared by particle lithography. (b) Nanopores were filled with a precursor solution of yttrium and erbium salts and dried. (c) Organosilane template was removed by heating to produce erbium-doped yttria nanoparticles.

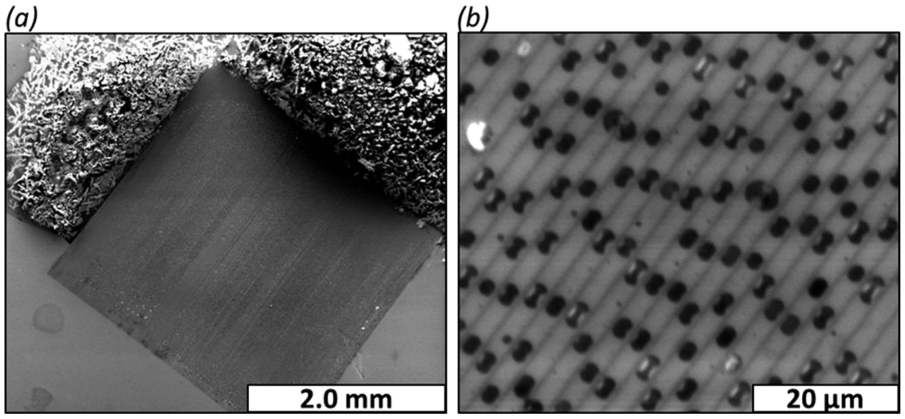

Figure 2. Microline surface structures of yttrium oxide prepared using capillary filling of PDMS molds shown with electron micrographs after calcination. (a) Microlines of yttrium oxide produced after heating. (b) Close-up view of the microparticles formed inside the PDMS mold.

reaction vessels were then immersed into a precursor solution of yttrium trichloroacetate doped with erbium cations (3%) for up to 3 h. The sample was removed slowly from the solution at a 90° angle to selectively fill the nanopores.[51] Upon drying, a tiny precipitate formed within each zeptoliter reaction vessel (Figure 1b). The sample was then heated at 150 °C to decompose the acetate to form $Y_2(CO_3)_3$ doped with 3% erbium. The temperature was then increased to 800 °C for 8 h for removal of CO_2 to produce nanosized rare earth oxides (Figure 1c). The same heating protocol developed for synthesis of micropatterns was used for preparing nanoparticles.

RESULTS AND DISCUSSION

Microline Patterns of Yttrium Oxide. The capillary filling approach for surface patterning was used successfully to prepare microparticles with an aligned arrangement as shown in Figure 2. The microstructures formed in line patterns were used to evaluate and optimize synthetic conditions (temperature, duration of heating and atmosphere requirements). The rectangular area of parallel lines indicates the region where the PDMS mold was placed, shown in the scanning electron micrographs in Figure 2. The overall area of Si(111) that was covered by the PDMS stamp is shown in Figure 2a. The dark square in the center of the image is the area where the PDMS mold was placed on top of the silicon wafer, and the buildup of material on either side of the square indicates where the drops of liquid were placed on the substrate for capillary filling. Within the square area, microline patterns were formed. When a drop of the liquid precursor solution was placed at the edge of the stamp, capillary forces drew the rare earth salt solution into the microchannels. As the sample dried, the salts formed line patterns of precipitates inside the channels, the remainder of the solution outside the PDMS stamp precipitated at the edge. After drying, the stamp was removed and the sample was heated to 800 °C to convert the yttrium salt to yttrium oxide. Microparticles that were produced within the channels after heating are shown in Figure 2b. The elongated shape of the microparticles is produced by the edges of the PDMS channels. Some of the particles reveal a coalescence of two particles within the microchannels to produce larger microparticles. Additional views of the microparticles acquired with AFM are shown in Figure S2 of the Supporting Information.

There are several advantages for the strategy of microfluidic filling of PDMS molds. Small volumes (less than 10 μL) of dilute reagent solutions can be used to pattern samples (1 × 1 cm^2). Also, the PDMS molds can be washed and recycled for preparing replicate samples. The simple steps for micropatterning require little time for preparation, so that multiple samples can be prepared for tuning heating parameters. Changes of the temperature, ramping steps, duration, and cooling for heating the precursor samples will alter the crystallization process and influence the shape (primary face growth), crystallinity and orientation. The heating step also provides a means to remove impurities. These factors become more significant as the dimensions are reduced to progressively smaller dimensions at the scale of nanometers.

Preparation and Analysis of Bulk Y_2O_3:Er. Powder X-ray diffraction and fluorescence measurements were done with a bulk sample of Y_2O_3:Er prepared in the same way as the nanoparticles, due to the inherent difficulty of analyzing trace quantities of nanoparticles. A precursor solution of erbium-doped yttrium trichloroacetate was dehydrated at 100 °C. The sample was then exposed to the same heat treatment used to form the nanoparticles (300 °C for 3 h followed by 800 °C for 8 h) producing a bulk sample of Y_2O_3:Er.

Powder X-ray diffraction data was collected with a Rigaku Ultima IV diffractometer with a Cu Kα source (λ = 1.54056 Å) and a DTex detector. The diffraction pattern for the erbium-doped yttrium trichloroacetate precursor before and after heating is shown in Figure 3. After heating, the diffraction

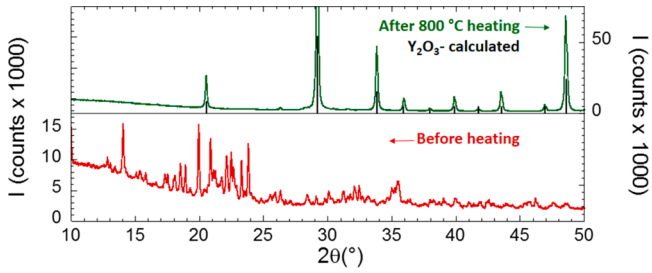

Figure 3. After heating the sample, yttrium oxide was formed. Powder X-ray diffraction spectra of erbium-doped yttrium trichloroacetate precursor (bottom) and the post-heat treatment Y_2O_3:Er (top).

pattern indexes to the calculated pattern for Y_2O_3. The sharp diffraction peaks indicate that the 800 °C heat treatment was sufficient to form highly crystalline Y_2O_3:Er from erbium-doped yttrium trichloroacetate.

To confirm the erbium doping of the Y_2O_3 sample, fluorescence measurements were conducted with a PerkinElmer LS 55 fluorescence spectrometer, shown in Figure 4. The fluorescence emission spectra (Ex = 384 nm) displays the four

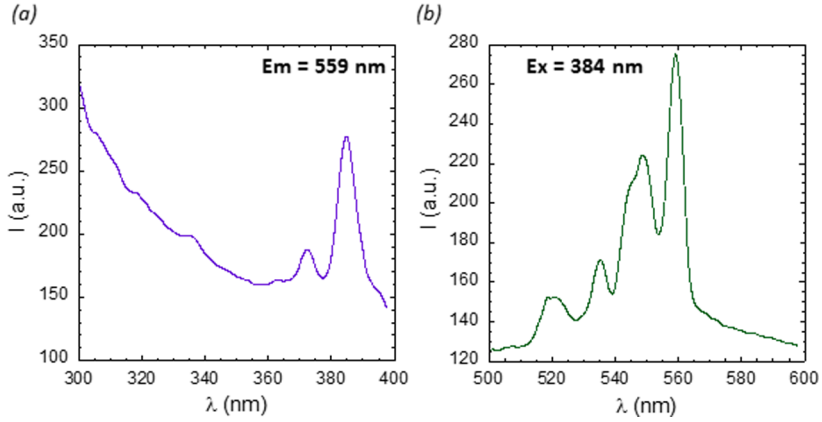

Figure 4. Emission spectrum of the bulk sample revealing the four characteristic transitions of Er^{3+}. (a) Fluorescence excitation spectrum (Em = 559 nm) and (b) emission spectrum (Ex = 384 nm).

emissions (521, 535, 549, and 559 nm) typical of Y_2O_3:Er due to the $^4S_{3/2} \rightarrow {}^4I^{15/2}$ transition in Er^{3+}, which is consistent with previously published spectra.[52]

Zeptoliter Reaction Vessels. For our approach based on particle lithography, a surface mask of silica mesospheres was used to define the surface coverage of organosilane resists. Monodisperse spherical particles self-assemble on flat surfaces to form periodic structures with designed dimensions and interparticle spacing, which provide a surface mask to define the sites for depositing organosilanes. With particle lithography, billions of nanostructures can be prepared on surfaces with relatively few defects and high reproducibility using basic steps of bench chemistry (mixing, centrifuging, heating, and drying). Silica mesoparticles with a diameter of 500 nm were used to prepare the organosilane nanopores shown in Figure 5. Measurements with AFM reveal that the spacing between the nanopores measures 505 ± 35 nm, which closely matches the diameter of the silica mesoparticles used as surface masks. The depth of the nanopores measured 1.4 ± 0.1 nm. The long-range order and periodicity of the nanopores formed on a silicon surface is evident in a representative topography view in Figure 5a. A map of the differences in chemistry between the methyl-terminated OTS film and areas exposed on the silicon substrate is shown with the simultaneously acquired lateral force image of Figure 5b. The diameter of the exposed sites of the substrate measured 90 ± 12 nm (n = 75), based on measurements from the lateral force frames. At the nanoscale, there are imperfections in the shapes of the nanopores (Figure 5b). A close-up view of the shapes and sizes of the nanopores is presented in Figure 5c. Details for a single nanopore are shown in Figure 5d (200 × 200 nm^2). Each nanopore was used as a reaction vessel to synthesize individual nanoparticles. Based on size measurements with AFM, the volume of a nanopore measures 1 × 10^{-21} L.

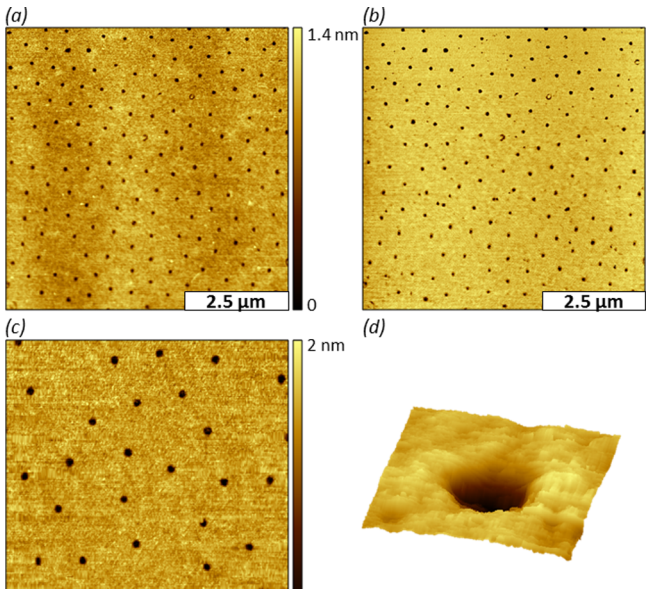

Figure 5. Nanopores within an OTS film produced with immersion particle lithography on Si(111). (a) Contact-mode topograph acquired in air; (b) concurrently acquired lateral force frame for a. (c) zoom-in view; (d) single nanopore within a 200 × 200 nm^2 topography frame.

The arrangement and spacing between nanoparticles is determined by the diameter of the silica particles used to fabricate the mask. The surface density of the patterned nanopores can be changed by choosing the diameter of the mesosphere mask. The height of the nanopores is determined by the thickness of the OTS film, which has an expected height of 2.6 nm for a densely pack film.[53,54] The nature of the substrate, solvent, concentration, temperature and immersion parameters must be optimized to achieve thicker films of OTS.[55] Imperfections at the nanoscale influence the volume of the nanopore reaction vessels. The size, geometry, and dispersity of the synthesized yttria nanoparticles will accordingly be influenced by the flaws in the substrate.

In the next step, the OTS nanopores were filled with the solution of precursor salt. The methyl-terminated film of OTS provided a resist to prevent nonspecific adsorption in areas surrounding the nanopores. After the sample was dried, precipitates formed inside the nanopores (Figure 6). A small bright dot can be detected within each nanopore surrounded by a protective matrix film of OTS. The surface of OTS surrounding the deposits is slightly rougher, indicating that small residues of the precursor salts persist on the matrix. Nanocrystals are readily identified within the nanopores from the representative height profiles in Figure 6b. A small hill was formed in the center of each nanopore where the dried salt residues formed a deposit. A single reaction vessel filled with a precipitate of yttria trichloroacetic acid is shown in Figure 6c. The edges of the OTS nanopores define a clear boundary surrounding the deposited salt. The height of the nanodeposits within the nanopores measured 1.4 ± 0.4 nm, however the

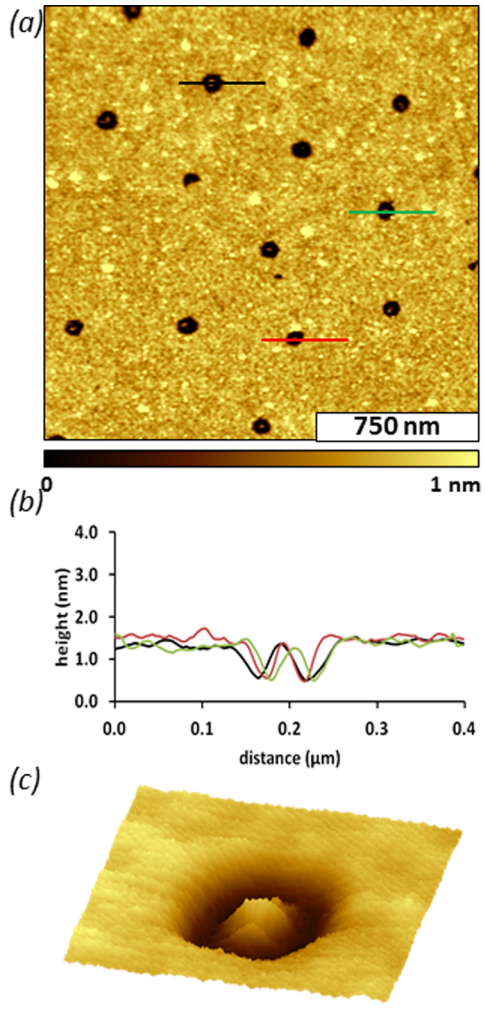

Figure 6. Zeptoliter vessels that were filled with rare earth precursor solution and dried. (a) Contact-mode topograph acquired in air; (b) height profile for the cursor lines in a. (c) Magnified view of a single salt deposit (200 × 200 nm^2).

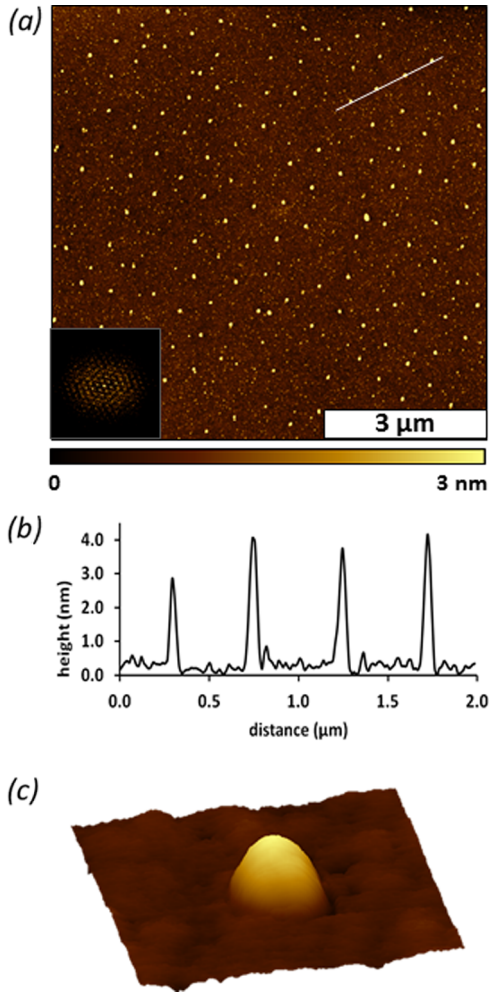

Figure 7. Surface arrangement of erbium-doped Y_2O_3 nanoparticles produced by heating. (a) Topography image acquired with tapping-mode AFM in air. The inset is the corresponding FFT. (b) Height profile for the white line in a. (c) Magnified topography view (200 × 200 nm^2) of an individual nanoparticle.

baselines at the edges of the nanostructures that were used for AFM cursor measurements likely did not reach the substrate. The areas surrounding the deposits may be partially filled with salts.

Within the representative AFM views of Figure 6, the OTS film was an effective resist for preventing attachment of the salts in areas surrounding the nanopores. The nanopores with OTS were filled with the salt solution and the periodic arrangement enables isolation to prevent aggregation when the sample is heated at high temperature. A similarly prepared sample was made using an organosilane terminated with polyethylene glycol groups. The PEG-silane film was not an effective resist for depositing precursor salts; the sample showed deposits located on areas throughout the sample.

The sample of dried salt deposits shown in Figure 6 was heated to 800 °C to produce an array of well-defined nanoparticles on Si(111). During the heating steps, the salt mixture is restructured into nanocrystals of erbium-doped yttria (Figure 7). At high temperatures, the organic film of OTS was removed by calcination. The spacing between the nanoparticles measured 490 ± 37 nm, which corresponds to the diameter of the silica mesospheres used as a surface mask. The example of Figure 7 is representative of the high-throughput capabilities of particle lithography for patterning and arranging nanomaterials. Within the 7 × 7 μm^2 view there are ~140 nanoparticles, which scales to a surface density of 1 × 10^8 nanoparticles per cm^2. There appears to be small residues in a few areas between the nanoparticles, which most likely are residual salts that attached to OTS. The corresponding FFT of the AFM topography image is presented in the inset of Figure 7a, and reflects the periodicity of the sample. Height measurements of four nanoparticles are shown in Figure 7b. The nanoparticles range in height from 1 to 4 nm, with the average height measuring 3.8 ± 1.1 nm (n = 66). A single nanoparticle is shown in Figure 7c, evidencing clean removal of the OTS film. To test the effect of increased soaking time, another sample was prepared in which the OTS nanopores were immersed for 3 h in the saturated solution (see the Supporting Information, Figure S3). After heating, the height of nanoparticles prepared with longer immersion measured 3.1 ± 0.9 nm (n = 86). Because there was no apparent increase in the size of nanoparticles, we concluded that 1 h of immersion was sufficient for filling the nanopores.

The heating process provides a means to obtain the desired product and remove organic contaminants. During heating, the yttrium salt deposited within the nanopores was converted to

yttrium oxide according to the XRD characterizations of a bulk sample prepared under identical heating conditions (Figure 3). When samples are heated to high temperatures, there is a possibility of sintering and aggregation of the deposits. The OTS film prevented aggregation of the nanoparticles during the heating step and was removed completely by calcination at high temperatures. An OTS SAM has been reported to degrade at temperatures starting at 200 °C and is no longer evident at temperatures of ∼480 °C according to thermogravimetric analysis.[56] The nature of the substrate is an important consideration for surface-directed synthesis, polished silicon wafers were used in this example. Organosilane SAMs provide flexibility for using substrates such as glass, indium tin oxide, quartz or silicon wafers, which can sustain synthetic steps at high temperatures.

The effect of the salt concentrations in the rare earth solution was tested to evaluate changes in nanoparticle size using a 50% reduction in concentration (see the Supporting Information, Figure S3). After soaking for 1 h at 0.05 M concentration, we were unable to locate nanoparticles on the silicon substrate. However, nanoparticles were produced when the immersion time was increased to 3 h. The average height of the nanoparticles produced with lower salt concentration measured 0.5 ± 0.1 nm (n = 27). At reduced concentration, the sizes of the nanoparticles were much smaller than those prepared from the saturated solution, using the same platform and dimensions of OTS nanopores as reaction vessels. We are currently investigating the potential of other resist films to use for high temperature synthesis of REO nanoparticles. We anticipate that surface designs with deeper pores will produce larger nanoparticles.

The proximity of neighboring nanoparticles can influence surface properties according to the distance or spacing between adjacent materials. Patterning inorganic materials by surface-templated reactions on small regions of a surface is not a conventional approach for inorganic synthesis. Factors such as dilution, contamination, and reproducibility become increasingly significant as the dimensions are reduced. As the spacing between reaction vessels becomes smaller it is possible that aggregation could occur. Future directions for surface-directed synthesis of REO nanomaterials will evaluate if there are spatial limits for the spacing between nanopores. The surface-directed strategy can be extended to other REO and oxide nanoparticles which require processing at high temperatures to effect crystallization. Designed surface arrangements with periodic spacing will facilitate measurements with individual, discrete crystals with defined surface density and arrangements. In future studies, the catalytic, magnetic, and photophysical properties of the arrays of nanoparticles will be examined as a function of nanoparticle size using scanning probe microscopies and surface spectroscopies.

CONCLUSIONS

We have developed approaches for surface-directed synthesis to prepare microstructures and nanostructures of REO materials. Conventional wet chemistry approaches are not suitable for preparing nanoparticles of rare earth oxides because relatively high temperatures are required that exceed the typical range of boiling solvents. Microstructures were used to evaluate and optimize synthetic conditions for advancing to smaller nanostructures, (e.g., temperature, duration of heating and atmosphere requirements). With particle lithography, nanopores within an organosilane matrix film were generated from a mask of monodisperse silica beads on Si(111). The nanopores were used as zeptoliter-sized reaction vessels to define the sites for surface-directed synthesis. The nanostructured film of organosilanes provided a sacrificial template, which is destroyed when surfaces are heated to high temperatures. However, the arrangement of inorganic deposits persists after heating, and becomes restructured into crystalline nanomaterials. Small volumes of dilute solutions were used to synthesize nanoparticles over areas spanning several centimeters. Because the approach is based on surface masks of mesospheres, the erbium-doped yttria nanoparticles were synthesized to yield well-defined arrangements conforming to the periodic packing of silica beads.

ASSOCIATED CONTENT

Supporting Information

Additional figures and information. This material is available free of charge via the Internet at http://pubs.acs.org.

AUTHOR INFORMATION

Corresponding Author

*E-mail: jgarno@lsu.edu. Phone: 225-578-8942. Fax: 225-578-3458. Address: Chemistry Department, Louisiana State University, 232 Choppin Hall, Baton Rouge, LA 70803.

Notes

The authors declare no competing financial interest.

ACKNOWLEDGMENTS

The authors gratefully acknowledge financial support from the Office of Basic Energy Sciences, U.S. Department of Energy (DE-FG02-08ER46528), the National Science Foundation Career/PECASE award (CHE-0847291), the American Chemical Society Petroleum Research Fund (New Directions 52305-ND), and the Dreyfus Foundation (Camille-Dreyfus Teacher-Scholar Award). Research reported in this publication was partially supported by the NIGMS of the NIH under Award Number R25GM069743.

REFERENCES

(1) Ronda, C. R.; Jüstel, T.; Nikol, H. Rare earth phosphors: Fundamentals and applications. *J. Alloys Compd.* **1998**, *275−277* (0), 669−676.

(2) Trovarelli, A. Catalytic properties of ceria and CeO_2-containing materials. *Catal. Rev.: Sci. Eng.* **1996**, *38* (4), 439−520.

(3) Rosynek, M. P. Catalytic properties of rare-earth oxides. *Catal. Rev.: Sci. Eng.* **1977**, *16* (1), 111−154.

(4) Koehler, W. C. Magnetic properties of rare-earth metals and alloys. *J. Appl. Phys.* **1965**, *36* (3), 1078−1087.

(5) Nesbitt, E. A. New permanent magnet materials containing rare-earth metals. *J. Appl. Phys.* **1969**, *40* (3), 1259−1265.

(6) Yan, Z.-G.; Yan, C.-H. Controlled synthesis of rare earth nanostructures. *J. Mater. Chem.* **2008**, *18* (42), 5046−5059.

(7) Dosev, D.; Guo, B.; Kennedy, I. M. Photoluminescence of Eu^{3+}: Y_2O_3 as an indication of crystal structure and particle size in nanoparticles synthesized by flame spray pyrolysis. *J. Aerosol Sci.* **2006**, *37* (3), 402−412.

(8) Niu, Z.; Li, Y. Removal and utilization of capping agents in nanocatalysis. *Chem. Mater.* **2014**, *26* (1), 72−83.

(9) Thomson, T.; Lee, S. L.; Toney, M. F.; Dewhurst, C. D.; Ogrin, F. Y.; Oates, C. J.; Sun, S. Agglomeration and sintering in annealed FePt nanoparticle assemblies studied by small angle neutron scattering and X-ray diffraction. *Phys. Rev. B: Condens. Matter Mater. Phys.* **2005**, *72* (6), 0644411−0644417.

(10) Thalladi, V. R.; Whitesides, G. M. Crystals of crystals: Fabrication of encapsulated and ordered two-dimensional arrays of microcrystals. *J. Am. Chem. Soc.* **2002**, *124* (14), 3520−3521.
(11) Wang, L.; Lee, M. H.; Barton, J.; Hughes, L.; Odom, T. W. Shape-control of protein crystals in patterned microwells. *J. Am. Chem. Soc.* **2008**, *130* (7), 2142−2143.
(12) Aizenberg, J.; Black, A. J.; Whitesides, G. M. Control of crystal nucleation by patterned self-assembled monolayers. *Nature* **1999**, *398* (6727), 495−498.
(13) Zhong, Z. Y.; Gates, B.; Xia, Y. N.; Qin, D. Soft lithographic approach to the fabrication of highly ordered 2D arrays of magnetic nanoparticles on the surfaces of silicon substrates. *Langmuir* **2000**, *16* (26), 10369−10375.
(14) Lyles, B. F.; Terrot, M. S.; Hammond, P. T.; Gast, A. P. Directed Patterned Adsorption of Magnetic Beads on Polyelectrolyte Multilayers on Glass. *Langmuir* **2004**, *20*, 3028−3031.
(15) Ma, R.; Lu, N.; Liu, L.; Wang, Y.; Shi, S.; Chi, L. Fabrication of Single Gold Particle Arrays with Pattern Directed Electrochemical Deposition. *ACS Appl. Mater. Interfaces* **2012**, *4*, 3779−3783.
(16) Li, J. R.; Garno, J. C. Elucidating the role of surface hydrolysis in preparing organosilane nanostructures via particle lithography. *Nano Lett.* **2008**, *8* (7), 1916−1922.
(17) Li, J. R.; Lusker, K. L.; Yu, J. J.; Garno, J. C. Engineering the spatial selectivity of surfaces at the nanoscale using particle lithography combined with vapor deposition of organosilanes. *ACS Nano* **2009**, *3* (7), 2023−2035.
(18) Saner, C. K.; Lusker, K. L.; LeJeune, Z. M.; Serem, W. K.; Garno, J. C. Self-assembly of octadecyltrichlorosilane: Surface structures formed using different protocols of particle lithography. *Beilstein J. Nanotechnol.* **2012**, *3*, 114−122.
(19) Mullen, T. J.; Zhang, M.; Feng, W.; El-khouri, R. J.; Sun, L.-D.; Yan, C.-H.; Patten, T. E.; Liu, G.-y. Fabrication and characterization of rare-earth-doped nanostructures on surfaces. *ACS Nano* **2011**, *5* (8), 6539−6545.
(20) Wang, S.; Sobczynski, D. J.; Jahanian, P.; Xhahysa, J.; Mao, G. A Supra-monolayer Nanopattern for Organic Nanoparticle Array Deposition. *ACS Appl. Mater. Interfaces* **2013**, *5*, 2699−2707.
(21) Mao, Y.; Guo, X.; Tran, T.; Wang, K. L.; Shih, C. K.; Chang, J. P., Luminescent properties of ensemble and individual erbium-doped yttrium oxide nanotubes. *J. Appl. Phys.* **2009**, *105*−*108* (9).
(22) Pires, A. M.; Serra, O. A.; Heer, S.; Gudel, H. U., Low-temperature upconversion spectroscopy of nanosized Y_2O_3: Er,Yb phosphor. *J. Appl. Phys.* **2005**, *98*−*104* (6).
(23) Fard, H. R.; Becker, N.; Hess, A.; Pashayi, K.; Proslier, T.; Pellin, M.; Borca-Tasciuc, T., Thermal conductivity of Er^{+3}:Y_2O_3 films grown by atomic layer deposition. *Appl. Phys. Lett.* **2013**, *103*−*107* (19).
(24) Eilers, H. Synthesis and characterization of nanophase yttria co-doped with erbium and ytterbium. *Mater. Lett.* **2006**, *60* (2), 214−217.
(25) Hyppanen, I.; Holsa, J.; Kankare, J.; Lastusaari, M.; Pihlgren, L. Up-conversion luminescence properties of Y_2O_2S:Yb^{3+},Er^{3+} nanophosphors. *Opt. Mater.* **2009**, *31* (12), 1787−1790.
(26) Capobianco, J. A.; Vetrone, F.; D'Alesio, T.; Tessari, G.; Speghini, A.; Bettinelli, M. Optical spectroscopy of nanocrystalline cubic Y_2O_3: Er^{3+} obtained by combustion synthesis. *Phys. Chem. Chem. Phys.* **2000**, *2* (14), 3203−3207.
(27) Anh, T. K.; Minh, L. Q.; Vu, N.; Huong, T. T.; Huong, N. T.; Barthou, C.; Strek, W. Nanomaterials containing rare-earth ions Tb, Eu, Er and Yb: preparation, optical properties and application potential. *J. Lumin.* **2003**, *102*, 391−394.
(28) Capobianco, J. A.; Vetrone, F.; Boyer, J. C.; Speghini, A.; Bettinelli, M. Enhancement of red emission ($^4F_{9/2}$ −> $^4I_{15/2}$) via upconversion in bulk and nanocrystalline cubic Y_2O_3: Er^{3+}. *J. Phys. Chem. B* **2002**, *106* (6), 1181−1187.
(29) Yin, S.; Shinozaki, M.; Sato, T. Synthesis and characterization of wire-like and near-spherical Eu_2O_3-doped Y_2O_3 phosphors by solvothermal reaction. *J. Lumin.* **2007**, *126* (2), 427−433.
(30) Chandra, S.; Deepak, F. L.; Gruber, J. B.; Sardar, D. K. Synthesis, morphology, and optical characterization of nanocrystalline Er^{3+}:Y_2O_3. *J. Phys. Chem. C* **2010**, *114* (2), 874−880.
(31) Wang, X.; Li, Y. D. Rare-earth-compound nanowires, nanotubes, and fullerene-like nanoparticles: Synthesis, characterization, and properties. *Chem.—Eur. J.* **2003**, *9* (22), 5627−5635.
(32) Fang, Y. P.; Xu, A. W.; You, L. P.; Song, R. Q.; Yu, J. C.; Zhang, H. X.; Li, Q.; Liu, H. Q. Hydrothermal synthesis of rare earth (Tb, Y) hydroxide and oxide nanotubes. *Adv. Funct. Mater.* **2003**, *13* (12), 955−960.
(33) Mao, J.; Huang, R.; Ostroumov, K. L.; Wang, J. P.; Chang, J. Synthesis and Luminescence Properties of Erbium-Doped Y_2O_3 Nanotubes. *J. Phys. Chem. C* **2008**, *112*, 2278−2285.
(34) De, G. H.; Qin, W. P.; Zhang, J. S.; Zhang, J. H.; Wang, Y.; Cao, C. Y.; Cui, Y. Upconversion luminescence properties of Y_2O_3: Yb^{3+}, Er^{3+} nanostructures. *J. Lumin.* **2006**, *119*, 258−263.
(35) Tang, Q.; Liu, Z. P.; Li, S.; Zhang, S. Y.; Liu, X. M.; Qian, Y. T. Synthesis of yttrium hydroxide and oxide nanotubes. *J. Cryst. Growth* **2003**, *259* (1−2), 208−214.
(36) Zhenxiu, X.; Zhanglian, H.; Qichao, Z.; Lixia, P.; Pengyue, Z. Preparation and luminescence properties of Y_2O_3: Eu^{3+} nanorods via post annealing process. *J. Rare Earths* **2006**, *24* (1, Supplement 1), 111−114.
(37) Nelson, J. A.; Brant, E. L.; Wagner, M. J. Nanocrystalline Y_2O_3: Eu phosphors prepared by alkalide reduction. *Chem. Mater.* **2003**, *15* (3), 688−693.
(38) Wu, G. S.; Lin, Y.; Yuan, X. Y.; Xie, T.; Cheng, B. C.; Zhang, L. D. A novel synthesis route to Y_2O_3:Eu nanotubes. *Nanotechnology* **2004**, *15* (5), 568−571.
(39) Pang, Q.; Shi, J. X.; Liu, Y.; Xing, D. S.; Gong, M. L.; Xu, N. S. A novel approach for preparation of Y_2O_3: Eu^{3+} nanoparticles by microemulsion-microwave heating. *Mater. Sci. Eng., B* **2003**, *103* (1), 57−61.
(40) Lee, M. H.; Oh, S. G.; Yi, S. C. Preparation of Eu-doped Y_2O_3 luminescent nanoparticles in nonionic reverse microemulsions. *J. Colloid Interface Sci.* **2000**, *226* (1), 65−70.
(41) Hirai, T.; Orikoshi, T.; Komasawa, I. Preparation of Y_2O_3: Yb,Er infrared-to-visible conversion phosphor fine particles using an emulsion liquid membrane system. *Chem. Mater.* **2002**, *14* (8), 3576−3583.
(42) Venkatachalam, N.; Yamano, T.; Hemmer, E.; Hyodo, H.; Kishimoto, H.; Soga, K. Er^{3+} -Doped Y_2O_3 nanophosphors for near-infrared fluorescence bioimaging applications. *J. Am. Ceram. Soc.* **2013**, *96* (9), 2759−2765.
(43) Silver, J.; Martinez-Rubio, M. I.; Ireland, T. G.; Fern, G. R.; Withnall, R. The effect of particle morphology and crystallite size on the upconversion luminescence properties of erbium and ytterbium co-doped yttrium oxide phosphors. *J. Phys. Chem. B* **2001**, *105* (5), 948−953.
(44) Zhang, J.; Wang, S. W.; Rong, T. J.; Chen, L. D. Upconversion luminescence in Er^{3+} doped and Yb^{3+}/Er^{3+} codoped yttria nanocrystalline powders. *J. Am. Ceram. Soc.* **2004**, *87* (6), 1072−1075.
(45) Rajasekharan, V. V.; Buttry, D. A. Electrochemical synthesis of yttrium oxide nanotubes. *Chem. Mater.* **2006**, *18* (19), 4541−4543.
(46) Yang, L.; Tang, Y.; Chen, X.; Li, Y.; Cao, X. Synthesis of Eu^{3+} doped Y_2O_3 nanotube arrays through an electric field-assisted deposition method. *Mater. Chem. Phys.* **2007**, *101* (1), 195−198.
(47) Dragoo, A. L.; Domingues, L. P. Preparation of high-density ceria-yttria ceramics. *J. Am. Ceram. Soc.* **1982**, *65* (5), 253−259.
(48) Patel, N.; Sanders, G. H. W.; Shakesheff, K. M.; Cannizzaro, S. M.; Davies, M. C.; Langer, R.; Roberts, C. J.; Tendler, S. J. B.; Williams, P. M. Atomic force microscopic analysis of highly defined protein patterns formed by microfluidic networks. *Langmuir* **1999**, *15* (21), 7252−7257.
(49) Delamarche, E.; Bernard, A.; Schmid, H.; Bietsch, A.; Michel, B.; Biebuyck, H. Microfluidic networks for chemical patterning of substrate: Design and application to bioassays. *J. Am. Chem. Soc.* **1998**, *120* (3), 500−508.
(50) Delamarche, E.; Bernard, A.; Schmid, H.; Michel, B.; Biebuyck, H. Patterned delivery of immunoglobulins to surfaces using microfluidic networks. *Science* **1997**, *276*, 779−781.

(51) Jackman, R. J.; Duffy, D. C.; Ostuni, E.; Willmore, N. D.; Whitesides, G. M. Fabricating large arrays of microwells with arbitrary dimensions and filling them using discontinuous dewetting. *Anal. Chem.* **1998**, *70* (11), 2280−2287.
(52) Ji, R.; Ye, Y.; Hu, X.; Fan, J.; Liu, E.; Zhang, Q.; Zhao, C.; Ye, S. The green-emitting fluorescence of nano Y_2O_3:Er^{3+} under different excitations. *Sci. China—Phys. Mech Astron.* **2012**, *55*, 1152−1157.
(53) Tillman, N.; Ulman, A.; Schildkraut, J. S.; Penner, T. L. Incorporation of phenoxy groups in self-assembled monolayers on trichlorosilane derivatives - Effects on film thickness, wettability, and molecular-orientation. *J. Am. Chem. Soc.* **1988**, *110* (18), 6136−6144.
(54) Wasserman, S. R.; Tao, Y. T.; Whitesides, G. M. Structure and reacitivity of alkylsiloxane monolayers formed by reactions of alkyl trichlorosilanes on silicon substractes. *Langmuir* **1989**, *5* (4), 1074−1087.
(55) Wen, K.; Maoz, R.; Cohen, H.; Sagiv, J.; Gibaud, A.; Desert, A.; Ocko, B. M. Postassembly chemical modification of a highly ordered organosilane multilayer: New insights into the structure, bonding, and dynamics of self-assembling silane monolayers. *ACS Nano* **2008**, *2* (3), 579−599.
(56) Kim, H. K.; Lee, J. P.; Park, C. R.; Kwak, H. T.; Sung, M. M. Thermal decomposition of alkylsiloxane self-assembled monolayers in air. *J. Phys. Chem. B* **2003**, *107* (18), 4348−4351.